Structural and vibrational properties of α-MoO_3 from van der Waals corrected density functional theory calculations

Hong Ding,[1] Keith G. Ray,[2] Vidvuds Ozolins,[3] and Mark Asta[1]
[1]*Department of Materials Science and Engineering, University of California, Berkeley, California, USA*
[2]*Department of Physics, University of California, Berkeley, California, USA*
[3]*Department of Materials Science and Engineering, University of California, Los Angeles, California, USA*
(Received 4 October 2011; published 17 January 2012)

Structural and vibrational properties of α-MoO_3 are studied employing two recently proposed methodologies for incorporating van der Waals (vdW) contributions in density functional theory (DFT) based calculations. The DFT-D2 [S. Grimme, J. Comput. Chem. **27**, 1787 (2006)] and optB88 vdW-DFT [J. Klimeš *et al.*, J. Phys.: Condens. Matter **22**, 022201 (2010)] methods are shown to give rise to increased accuracy in predicted lattice parameters, relative to conventional DFT methods. Calculated vibrational frequencies agree with measurements to within 5% and 10% for modes involving bonded and nonbonded interactions in this compound, respectively.

DOI: 10.1103/PhysRevB.85.012104 PACS number(s): 61.50.Lt, 61.66.Fn, 63.20.D−

The α-MoO_3 compound is a layered oxide that has attracted interest for a range of applications including catalysis,[1] cathode materials for lithium-ion batteries,[2] and electrochemical supercapacitors.[3] As shown in Fig. 1, the crystal structure of α-MoO_3 is composed of sheets of distorted, edge-shared MoO_6 octahedra. Each octahedron contains three symmetry-distinct oxygen ions, which occupy 4*c* Wyckoff positions in the *Pbnm* orthorhombic space group.[4] The MoO_3 sheets are stacked along the *b* lattice direction of the orthorhombic unit cell, and are weakly bonded across a region commonly referred to as the "van-der-Waals gap."

Due to the technological interest in α-MoO_3, it has been the topic of several previous theoretical studies, based on electronic density-functional theory (DFT) within the local density (LDA)[5] and generalized gradient (GGA) approximations,[6] GGA plus Hubbard-*U* corrections for onsite Coulomb interactions,[7] and Hartree-Fock (HF) with a DFT-based correction for electron correlation.[8] Theoretical calculations and x-ray photoemission experiments,[9] establish a mixed ionic and covalent character for the Mo-O bonding within the sheets, characterized by a strong degree of hybridization between Mo 4*d* and O 2*p* electrons.[10] The interactions between the MoO_3 sheets are governed by both electrostatic and van der Waals (vdW) contributions as discussed in Ref. 11.

Due to the fact that vdW interactions are not accurately described by traditional GGA and LDA calculations, the equilibrium spacing between the MoO_3 sheets is not accurately predicted by these methods (see below). For studies of the electronic-structure and bonding properties of α-MoO_3, a practical solution to this problem has been to fix the *b* lattice constant at the experimentally measured value.[7,9] This approach is not feasible, however, for computational studies of defects and processes where large variations in the interlayer spacing may arise. An example is lithium-ion intercalation, where variations in Li content are coupled with large expansions in the interlayer spacing.[12,13] For applications of this type, a method with computational efficiency comparable to DFT is required, which accurately characterizes both the equilibrium bond lengths and bond stiffnesses of the host α-MoO_3 compound. In the present work, we assess the accuracy of recently proposed vdW corrected DFT-based methods for this purpose, through a comparison between theoretical results and experimental measurements for equilibrium lattice constants, bond lengths, and vibrational frequencies.

Several approaches have been developed for describing van der Waals interactions within the framework of DFT.[14] In the present work, we focus on two classes of approaches that feature computational requirements comparable to traditional DFT methods. The first is the DFT-D approach[15] in which the contribution to the totally energy associated with dispersion interactions is described by a classical pair potential with the C_{ij}/R_{ij}^6 form. Three generations of the method have been developed,[16] using different approaches for calculating the C_{ij} coefficients. The first uses an average of empirical coefficients from different hybridization states for each atom, while in the second (DFT-D2), the PBE0 hybrid method[17] is used to obtain atomic ionization energies and polarizabilities in the determination of C_{ij}. In both methods, these coefficients are obtained from mixing rules, using values tabulated in terms of the chemical identity of the atoms *i* and *j* alone. The DFT-D3 method makes use of time-dependent DFT[16] to calculate the C_{ij} coefficients through the averaged dipole polarizability as a function of frequency. Furthermore, it interpolates between results for different local environments to capture differences due to bonding geometry. In this method, the C_{ij} coefficients are derived taking into account structural information as well as the chemical identity of the atoms.

The second class of approaches considered in this work is the so-called van der Waals density functionals (vdW-DF),[20] in which the vdW contribution to the total energy is described through modifications to the correlation energy functional within DFT. Specifically, the DFT exchange-correlation functional is divided into three parts: $E_{xc} = E_{lc} + E_{nl} + E_x$, where E_{lc} is a local correlation energy described within the local density approximation, E_{nl} is the nonlocal correlation energy, and E_x is a semilocal exchange functional. The E_{nl} contribution is given by the integral: $E_{nl} = \frac{1}{2}\int d\mathbf{r}d\mathbf{r}' n(\mathbf{r})\phi(\mathbf{r},\mathbf{r}')n(\mathbf{r}')$, over electron densities, n at $\mathbf{r}$ and $\mathbf{r}'$, multiplied by an integration kernel, ϕ, which is derived from the adiabatic-connection theorem through a series of approximations.[20] We consider three different exchange functionals for use with the vdW-DF approach, as reported in the literature. These are revPBE

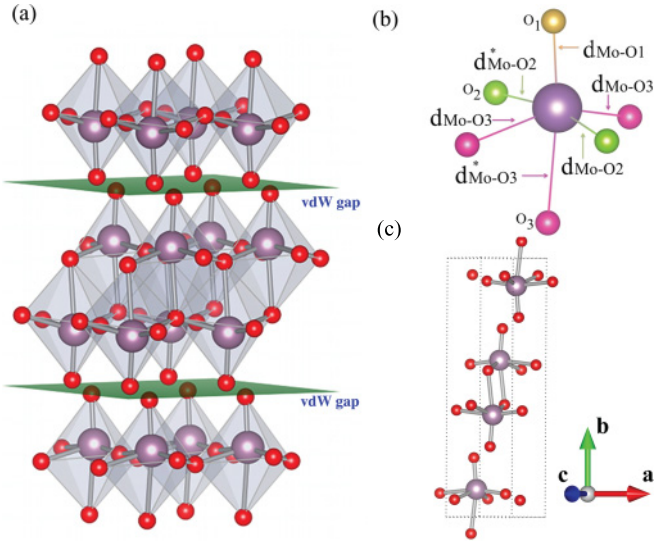

FIG. 1. (Color online) Structure of the orthorhombic α-MoO_3 compound. (a) Mo (purple) and O (red) octahedra are illustrated, as well as the vdW gap (green layer). (b) Symmetry-distinct oxygen ions in the MoO_6 octahedron are labeled O_1, O_2, and O_3. (c) The conventional unit cell.

TABLE I. A comparison of lattice constants (in the unit of Å) of α-MoO_3 calculated in the current and previous calculations, and measured experimentally. The asterisk superscript denotes calculated results where the b lattice parameter was fixed at the experimentally measured value.

Method		a	b	c
DFT	LDA[a]	3.729	13.036	3.478
	PW91[b]	3.965	14.673	3.721
	HF[c]	3.910	14.271	3.680
	PBE*[d]	4.023	13.855	3.755
DFT-D	DFT-D2	3.931	13.881	3.711
vdW-DF	vdW-DF	4.054	14.855	3.728
	vdW-DF2	4.043	14.691	3.753
	optB88	3.941	14.078	3.732
Expt.	Ref. 34 ($T = 300$ K)	3.962	13.860	3.697
	Ref. 35 ($T = 300$ K)	3.963	13.865	3.693
	Ref. 35 ($T \to 0$ K)	3.958	13.750	3.700

[a]Reference 5.
[b]Reference 6.
[c]Reference 8.
[d]Reference 9.

as in the original vdW-DF,[20] PW86 as in vdW-DF2,[21] and optB88,[22] a new exchange functional based on the B88 exchange functional.[23] RevPBE and optB88 are both paired with the same E_{nl}, while the E_{nl} used with PW86 has a changed parameter that relates how the length scale in E_{nl} is set by a corresponding GGA calculation. In vdW-DF2 and vdW-DF, this parameter comes from energy expansions appropriate for molecules or a slowly varying electron gas, respectively.

All the calculations performed in this work made use of the projector-augmented-wave (PAW) method,[24,25] as implemented in the Vienna *ab initio* simulation package (VASP).[26–29] The wave functions were expanded in a plane-wave basis with an energy cutoff of 600 eV. For calculations of the structure of the MoO_3 compound, we made use of the orthorhombic unit cell shown in Fig. 1(c), and sampled the Brillouin zone employing a $7 \times 5 \times 7$ mesh, using the Methfessel-Paxton scheme[30] with a smearing width of 0.1 eV. The PAW potentials employed in this work are those labeled "Mo" and "O" in the VASP PAW-PBE library. Internal coordinates were relaxed until energy and atomic forces converged to within 0.01 meV/atom and 0.005 eV $Å^{-1}$, respectively. The equilibrium lattice parameters were computed using conjugate-gradient minimization with the calculated stress tensors. Vibrational frequencies were obtained from a frozen-phonon approach. Based on several numerical tests, the convergence of the results presented below is estimated to be 0.02 Å for a and c, 0.05 Å for b, and within 6% for the vibrational frequencies.

For the DFT-D calculations, we employed the D2 method, with values of the dispersion coefficients (C_{ij}) given in Ref. 31, and a value of $s_6 = 0.75$. We also explored a modification of the DFT-D2 method, in which we employed Grimme's DFT-D3 codes[16] to calculate the C_{ij} coefficients, based on the experimentally determined geometry of the α-MoO_3 compound. These coefficients were then used in the VASP DFT-D2 implementation with $s_6 = 1$ as in DFT-D3 for the $n = 6$ two-body interaction.[16] This modified DFT-D2 method led to a decreased level of agreement with experiment relative to the original D2 method and will not be discussed further. In the vdW-DF calculations, we employed the VASP implementation developed by Klimeš *et al.*,[32] which makes use of an algorithm for efficiently evaluating the integral for E_{nl} due to Pérez and Soler.[33]

Table I compares the current results for the equilibrium lattice constants with those obtained by DFT-based approaches in previous calculations and experimental measurements. The temperature-dependent experimental data reported in Ref. 35 shows an anomalously large thermal expansion coefficient for the b lattice parameter. In what follows, we will therefore assess the level of agreement between experiment and theory using the extrapolations of the measured lattice constant values to zero temperature presenting in Ref. 35. The LDA results, taken from Ref. 5, feature theoretical lattice constants that are smaller than these measured values by 6% for a and c, and about 5% for b, respectively. For calculations where the value of the b lattice constant is unconstrained, it is seen that GGA (PW91) predicts values for a and c that agree to within 1% of the measured values, while the calculated b lattice constant is roughly 7% larger. The Hartree-Fock based results from Ref. 8 give values that are 1% and 0.5% smaller than measured values for a and c, and 4% larger for b, respectively. Thus the previous LDA, GGA, and HF calculations give rise to predictions for the interlayer spacing that are accurate to no better than 4% in comparison with experimental measurements.

We consider next the vdW-corrected DFT results obtained here. The PBE-based DFT-D2 method is seen to provide an excellent level of agreement with experiment for each of the three lattice constants, with the calculated values being 0.5% larger for a, 0.3% larger for c, and 1% larger for b. The vdW-DF results are found to vary significantly between the original vdW-DF implementation and the vdW-DF2 and

TABLE II. Calculated Mo-O bond lengths (in units of Å) obtained by the DFT-D2 and optB88 methods are compared with previous calculations and experimental results. The labeling of the bonds in the first column corresponds to the notation introduced in Fig. 1(c).

	DFT-D2	optB88	PBE[a]	Expt.[b]	Expt.[c]
$d_{Mo\text{-}O1}$	1.702	1.705	1.703	1.68	1.63
$d_{Mo\text{-}O2}$	1.771	1.778	1.761	1.74	1.74
$d^{*}_{Mo\text{-}O2}$	2.187	2.188	2.278	2.25	2.24
$d_{Mo\text{-}O3}$	1.954	1.964	1.975	1.95	1.96
$d^{*}_{Mo\text{-}O3}$	2.397	2.394	2.340	2.31	2.30

[a]Reference 9.
[b]Reference 34.
[c]Reference 35.

optB88 parametrizations. The original vdW-DF functional gives lattice constants that are uniformly larger than the measured values, by 1%, 4%, and 0.7% for a, b, and c, respectively. The vdW-DF2 approach leads to a slightly worse prediction for each of the lattice constants relative to the original vdW-DF. Of the three vdW-DFs considered in this work, the best level of agreement between experiment and calculations is obtained with the optB88 functional. This approach gives rise to predictions for a and c within 0.8% of measurements, and the b lattice constant is 2% larger than the experimental value. The improved accuracy of the optB88 functional obtained here for α-MoO_3 is similar to that found for metallic, covalent, and ionically bonded solids in Ref. 32, where the improvements of the optB88 functional for solids relative to the original vdW-DF and vdW-DF2 methods is attributed to a smaller exchange enhancement factor for small reduced gradients.

Overall, the best level of agreement between experiment and theory for the lattice constants is obtained with the DFT-D2 and optB88 vdw-DF methods. In what follows, we further assess the accuracy of these two methods, focusing on results for bond lengths and vibrational frequencies. Table II lists the bond lengths obtained from the present calculations, previous calculations,[9] and experimental measurements. The results obtained by the DFT-D2 and vdW-DF methods show excellent agreement with available experimental data, as well as previous PBE calculations, with the exception of $d^{*}_{Mo\text{-}O_2}$ and $d^{*}_{Mo\text{-}O_3}$ where the vdW-corrected calculations are smaller and larger than measurements by approximately 0.06 and 0.09 Å, respectively.

We consider next a comparison of calculated and experimentally measured vibrational frequencies. A comparison between the present calculations and measured values for the frequencies of the infrared and Raman-active modes presented in Ref. 39 shows average agreement at the level of 3% for both DFT-D2 and optB88 methods. In Table III, we give representative comparisons for the stretching modes of Mo-O bonds (first three rows), as well as the modes illustrated in Fig. 2, involving O-O bonds across the vdW gap. As shown in Table III, the DFT-D2 method overestimates the frequency of the Mo-O_1 stretching mode by about 1%, while giving predicted values of the Mo-O_2 and Mo-O_3 stretching modes that are about 3% smaller than measurements. In comparison, the optB88 method gives rise to predictions of

TABLE III. Experimentally measured vibrational frequencies (in units of cm^{-1}) in α-MoO_3 are compared to calculated results obtained with the DFT-D2 and optB88 methods. The first three rows list the Mo-O bond stretching vibrations and the next two the interlayer interaction vibration frequencies. The labels for the modes are taken from Ref. 36.

Symmetry	Assignment	DFT-D2	optB88	Expt.[a]	Expt.[b]	Expt.[c]
A_{1g}	$\upsilon O = Mo$	1006	996	996	–	–
B_{1g}	υOMo_2	801	796	820	–	–
B_{3g}	υOMo_3	640	632	666	–	–
B_{2u}	Lattice	54	63	–	58	53
B_{3u}	modes	50	42	–	46	44

[a]Reference 37.
[b]Reference 36.
[c]Reference 38.

Mo-O_1 stretching mode that are in good agreement with the most recent experiment,[37] and the Mo-O_2 and Mo-O_3 stretching modes are about 3 and 5% smaller than the experimental observations, respectively. Similar calculations have been performed within the GGA + U framework,[7] where calculated frequencies for the three Mo-O stretching modes are reported as 1023, 898, and 711 cm^{-1}, respectively.

The strength of the nonbonded interactions between the sheets can be assessed through the frequencies of the two modes illustrated in Fig. 2. These are referred to as the lattice mode (B_{2u}) and rigid-layer mode (B_{3u}) by Py and Maschke.[36] The lattice mode has partial shear character, but the rigid-layer mode involves only relative displacements that are normal to the vdW gap. Both modes probe the strength of the force constants between ions spanning the vdW gap. The computed vibrational frequencies based on DFT-D2 and optB88 methods are shown in Table III to agree with experimental measurements to within 10%.[36,38] This is an encouraging level of accuracy, suggesting that the DFT-D2 and optB88 methods represent reasonably well the competition between electrostatic and vdW forces underlying the interatomic interactions across the vdW gap in α-MoO_3.

To demonstrate the utility of the vdW-corrected DFT approaches more broadly, we end with results for the effect of Li-ion intercalation on the lattice constants in α-MoO_3. Li-ion intercalation into the vdW gap of α-MoO_3 leads to a pronounced expansion of the b lattice constant,[12,13] which can be sufficient to cause fracture of the host material. An important parameter for modeling such phenomena is the solute expansion coefficient $\alpha \equiv \partial \ln b/\partial x$, where x is the mole fraction of Li ions. Using the DFT-D2 and optB88 methods,

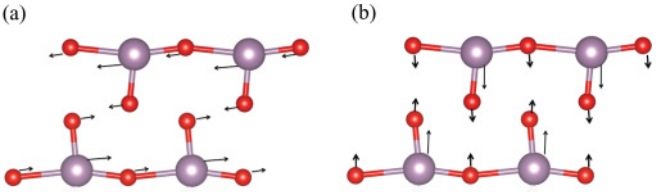

FIG. 2. (Color online) Two typical low-frequency vibration modes for α-MoO_3 between adjacent layers: (a) lattice mode (B_{2u}) and (b) rigid-layer mode (B_{3u}).

we obtain $\alpha = 0.51$ and 0.42, respectively. We emphasize that the calculation of intercalation-induced strains requires a method such as the vdW-corrected DFT methods considered here, which accurately describes the equilibrium bond lengths and force constants across the vdW gap.

In summary, vdW-corrected DFT methods have been applied to the calculation of the structure and vibrational frequencies of the α-MoO_3 compound. The DFT-D2 and optB88 methods yield calculated lattice parameters and bond lengths that agree with experimental measurements to within 0.8 and 1.6%, respectively. The calculated frequencies for stretching of Mo-O bonds agree with experimental measurements to within 5%, and for the modes that probe the force constants across the vdW gap, the frequencies are predicted with an accuracy of approximately ten percent. The present results show an encouraging level of accuracy in the application of vdW-corrected DFT methods for characterizing both bonded and nonbonded interatomic interactions in α-MoO_3.

This work was supported by the Molecularly Engineered Energy Materials Energy Frontier Research Center, funded by the US Department of Energy (DOE), Office of Science, Office of Basic Energy Sciences under award DE-SC0001342. This work made use of resources of the National Energy Research Scientific Computing Center, supported by the Office of Science of the US DOE under Contract No. DE-AC02-05CH11231.

[1] M. Labanowska, ChemPhysChem **2**, 712 (2001).
[2] J. S. Chen, Y. L. Cheah, S. Madhavi, and X. W. Lou, J. Phys. Chem. C **114**, 8675 (2010).
[3] T. Brezesinski, J. Wang, S. H. Tolbert, and B. Dunn, Nat. Mater. **9**, 146 (2010).
[4] H. C. Zeng, J. Cryst. Growth **186**, 393 (1998).
[5] M. Chen, U. V. Waghmare, C. M. Friend, and E. Kaxiras, J. Chem. Phys. **109**, 6854 (1998).
[6] X. Sha, L. Chen, A. C. Cooper, G. P. Pez, and H. Cheng, J. Phys. Chem. C **113**, 11399 (2009).
[7] R. Coquet and D. J. Willock, PhysChemChemPhys **7**, 3819 (2005).
[8] F. Cora, A. Patel, N. M. Harrison, C. Roetti, and C. R. A. Catlow, J. Mater. Chem. **7**, 959 (1997).
[9] D. O. Scanlon, G. W. Watson, D. J. Payne, G. R. Atkinson, R. G. Egdell, and D. S. L. Law, J. Phys. Chem. C **114**, 4636 (2010).
[10] A. B. Anderson, Y. Kim, D. W. Ewing, R. K. Grasselli, and M. Tenhover, Surf. Sci. **134**, 237 (1983).
[11] A. Sayede, T. Amriou, M. Pernisek, B. Khelifa, and C. Mathieu, Chem. Phys. **316**, 72 (2005).
[12] J. W. Bullard and R. L. Smith, Solid State Ionics **160**, 335 (2003).
[13] Y. Iriyama, T. Abe, M. Inaba, and Z. Ogumi, Solid State Ionics **135**, 95 (2000).
[14] A. Tkatchenko, L. Romaner, O. T. Hofmann, E. Zojer, C. Ambrosch-Draxl, and M. Scheffler, PhysChemChemPhys **35**, 435 (2010).
[15] S. Grimme, J. Comput. Chem. **25**, 1463 (2004).
[16] S. Grimme, J. Antony, S. Ehrlich, and H. Krieg, J. Chem. Phys. **132**, 154104 (2010).
[17] C. Adamo and V. Barone, J. Chem. Phys. **110**, 6158 (1999).
[18] J. P. Perdew, K. Burke, and M. Ernzerhof, Phys. Rev. Lett. **77**, 3865 (1996).
[19] J. P. Perdew, K. Burke, and M. Ernzerhof, Phys. Rev. Lett. **78**, 1396 (1997).
[20] M. Dion, H. Rydberg, E. Schröder, D. C. Langreth, and B. I. Lundqvist, Phys. Rev. Lett. **92**, 246401 (2004).
[21] K. Lee, E. D. Murray, L. Kong, B. I. Lundqvist, and D. C. Langreth, Phys. Rev. B **82**, 081101 (2010).
[22] J. Klimeš, D. Bowler, and A. Michaelides, J. Phys.: Condens. Matter **22**, 022201 (2010).
[23] A. D. Becke, Phys. Rev. A **38**, 3098 (1988).
[24] P. E. Blöchl, Phys. Rev. B **50**, 17953 (1994).
[25] G. Kresse and D. Joubert, Phys. Rev. B **59**, 1758 (1999).
[26] G. Kresse and J. Hafner, Phys. Rev. B **47**, 558 (1993).
[27] G. Kresse and J. Hafner, Phys. Rev. B **49**, 14251 (1994).
[28] G. Kresse and J. Furthmller, Comput. Mater. Sci. **6**, 15 (1996).
[29] G. Kresse and J. Furthmuller, Phys. Rev. B **54**, 11169 (1996).
[30] M. Methfessel and A. T. Paxton, Phys. Rev. B **40**, 3616 (1989).
[31] S. Grimme, J. Comput. Chem. **27**, 1787 (2006).
[32] J. Klimes, D. R. Bowler, and A. Michaelideš, Phys. Rev. B **83**, 195131 (2011).
[33] G. Roman-Pérez and J. M. Soler, Phys. Rev. Lett. **103**, 096102 (2009).
[34] H. Sitepu, Powder Diffr. **24**, 315 (2009).
[35] H. Negishi, S. Negishi, Y. Kuroiwa, N. Sato, and S. Aoyagi, Phys. Rev. B **69**, 064111 (2004).
[36] M. Py and K. Maschke, Physica B + C **105**, 370 (1981).
[37] J. V. Silveira, J. A. Batista, G. D. Saraiva, J. M. Filho, A. G. S. Filho, S. Hu, and X. Wang, Vib. Spectrosc. **54**, 179 (2010).
[38] G.-A. Nazri and C. Julien, Solid State Ionics **53–56,** part 1, 376 (1992).
[39] L. Seguin, M. Figlarz, R. Cavagnat, and J.-C. Lassgues, Spectrochimic. Acta Part A **51**, 1323 (1995).